On the stability of straight crack paths in brittle heterogeneous solids under mode I loading

M. ABDULMAJID[a], L. PONSON[b]

a. Institut Jean Le Rond d'Alembert,Université Pierre et Marie Curie, 75005 Paris, France
mohamad.abdulmajid@etu.upmc.fr
b. Institut Jean Le Rond d'Alembert, CNRS - Université Pierre et Marie Curie, 75005 Paris, France
laurent.ponson@upmc.fr

Abstract

The classical fracture mechanics approach describes only partially the fracture process in heterogeneous brittle materials-such as rocks, ceramics or concrete for example. The study of crack growth in weakly heterogeneous solids where fracture behaviors can be seen as a perturbation from the response of homogeneous media is a fruitful approach that provides rich insights on the role of heterogeneities on crack propagation.
In this work, we focus on the path followed by cracks, and study whether a crack previously disturbed by some heterogeneities recovers a straight trajectory or instead departs from it. To address this question, we build on the work of Cotterell and Rice [1] enriched by the one of Movchan et al. [2] to derive a path equation for a slightly perturbed crack under macroscopic mode I loading. This path equation is then used to investigate the stability of straight crack trajectories. Three regimes corresponding to different loading conditions that can be parametrized through two length scales emerging from the geometry of the fracturing sample and the loading conditions can be evidenced : (i) a stable regime where path perturbations rapidly decay (ii) an unstable regime with an exponential growth of the geometrical crack perturbations (iii) a marginally stable regime that displays oscillatory crack solutions. These predictions are compared with experimental fracture tests in various geometries where crack path disturbances are manually introduced. We find that our approach accounts for the stability of straight trajectory as observed experimentally. The conditions required to observe oscillatory crack paths are finally discussed.

Résumé

L'approche classique de la mécanique de la rupture ne décrit que partiellement le processus de rupture dans des matériaux fragiles hétérogènes, comme les roches, la céramique ou le béton, par exemple. L'étude de la propagation des fissures dans les solides faiblement hétérogènes où les comportements de rupture peut être perçue comme une perturbation de la réponse des milieux homogènes est une approche fructueuse qui fournit de riches aperçus sur le rôle des hétérogénéités sur la propagation des fissures.
Dans ce travail, nous nous concentrons sur la trajectoire suivie par les fissures et étudions si une fissure précédemment perturbée par certaines hétérogénéités récupère une trajectoire droite ou au contraire s'en écarte. Pour répondre à cette question, nous nous appuyons sur les travaux de Cotterell et Rice [1] enrichis par celui de Movchan et al. [2] pour dériver une équation de chemin pour une fissure légèrement perturbée sous chargement macroscopique de mode I. Cette équation de cheminement est ensuite utilisée pour étudier la stabilité des trajectoires de fissures droites. On peut mettre en évidence trois régimes correspondant à différentes conditions de charge paramétrables à travers deux échelles de longueur émergeant de la géométrie de l'échantillon et des conditions de chargement : (i) un régime stable où les perturbations de trajet décroissent rapidement (ii) un régime instable avec un croissance exponentielle des perturbations géométriques de fissure (iii) régime marginalement stable qui présente des solutions de fissuration oscillatoire.
Ces prédictions sont comparées à des essais expérimentaux de ruptures dans diverses géométries où les perturbations de la fissure sont introduites manuellement. Nous constatons que notre approche tient

compte de la stabilité de la trajectoire droite observée expérimentalement. Les conditions requises pour observer les chemins de fissures oscillatoires sont enfin discutées.

Keywords : Fracture-mechanics, crack path, stability analysis

1 Introduction

Crack path prediction is one of the main challenges in the field of fracture mechanics. The determination of crack propagation laws is necessary to describe the fracture phenomenon as a pattern formation process induced by mechanical stresses. Within the framework of Linear Elastic Fracture Mechanics (LEFM), the propagation of a crack is mainly governed by the singular behavior of the stress field in the vicinity of its tip.

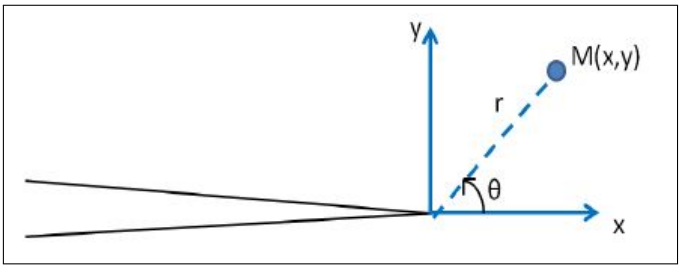

FIGURE 1 – Repère local en pointe de fissure

For a two-dimensional quasi-static crack, which is the main purpose of the presentwork, this behavior is given by

$$\begin{cases} \sigma_{xx} = \dfrac{K_I}{\sqrt{2\pi r}} + T + A\sqrt{r} \\ \sigma_{yy} = \dfrac{K_I}{\sqrt{2\pi r}} + A\sqrt{r} \end{cases} \tag{1}$$

where K_I is the stress intensity factor for mode I loading (SIF). The evolution of the crack tip is governed by the Griffith energy criterion, which states that the intensity of the loading necessary to induce propagation is given by G = Γ, where G is the energy release rate and Γ is the fracture energy of the material, that is the energy needed to create new free surfaces.

While this criterion is very useful in predicting crack initiation, it cannot predict the direction of the crack tip, and therefore in most cases it is not sufficient to determine the actual path of the crack. In order to achieve this, several suggestions have been made. Among them, the Principle of Local Symmetry (PLS) states that the crack advances in such a way that in-plane shear stress vanishes in the vicinity of the crack tip, or explicitly

$$K_{II} = 0 \tag{2}$$

To address the problem of crack path prediction, we will devise our work to two parts (analytical and experimental).

2 Analytical calculation

In order to predict the crack path, the local stress intensity factors must be expressed as a function of the crack geometry h (x). We use the results of Cotterel and Rice [1], enriched by the work of Movchan et al. [2], which provide k_I, k_{II}, the stress intensity factors after the crack tip as a function of h (x), macroscopic stress intensity factors K_I^0, $K_{II}^{(0)}$ before the crack tip, and the coefficients $T^{(0)}$,$A^{(0)}$ of higher order terms in the development of the stress field near the tip of a semi-infinite crack in an infinite elastic medium :

$$\begin{cases} k_I = K_I^{(0)} \\ k_{II} = K_{II}^{(0)} + \dfrac{K_I^{(0)}}{2}\dfrac{dh}{dx}_{x-} - \sqrt{\dfrac{\pi}{2}}A^{(0)}h(x) - \sqrt{\dfrac{2}{\pi}}T^{(0)}\displaystyle\int_{-\infty}^{x}\frac{h'(u)}{\sqrt{x-u}}du \end{cases} \tag{3}$$

We obtain the crack path equation using the local symmetry principle and assuming that a crack propagates along the mode of zero shear stress when the sample is subjected to pure traction. The geometrical perturbations of the crack profiles give some local non-zero shear-stress in the vicinity of the crack tip. Following the idea of Katzav et al. [3], we start from the calculation of Amestoy and Leblond [4], based on the principle of local symmetry, which predicts the direction of propagation θ, as a function of the value of the stress intensity factors :

$$\theta(x^+) = -2\frac{k_{II}(x)}{k_I(x)} \tag{4}$$

The angle θ is defined as the angle between the tangent to the trajectory in $x = x^-$ and the direction followed by the crack in $x = x^+$, as shown in Figure 1. The crack path is then approximated by a succession of rectilinear segments separated by an increment δx along the direction x which can be taken subsequently in the limit $\delta x \to 0$. Therefore, the $\theta(x^+)$ angle in the preceding equation provides for the propagation direction on the right side of x while the local stress intensity factors $k_I(x)$ and $k_{II}(x)$ are computed from the crack path configuration before propagation. We limit our study to cracks with small angles $\theta \ll 1$ as the experiments and the simulations, we have then $\theta(x^+) \approx \frac{dh}{dx}_{x+} - \frac{dh}{dx}_{x-}$.

Thus $K_{II}^{(0)} = 0$ then, equation 4 would be :

$$\boxed{\frac{dh}{dx} = \frac{2\sqrt{2}}{\sqrt{\pi}}\frac{T^{(0)}}{K_I^{(0)}}\int_{-\infty}^{x}\frac{h'(u)}{\sqrt{x-u}}du + \sqrt{2\pi}\frac{A_I^{(0)}}{K_I^{(0)}}h(x).} \tag{5}$$

We will define the length $\mathcal{L}_1$ as :

$$\mathcal{L}_1 = \frac{\pi}{8}(\frac{K_I}{T})^2 \tag{6}$$

And the length $\mathcal{L}_2$ as :

$$\mathcal{L}_2 = \frac{1}{\sqrt{2\pi}}(\frac{K_I}{A}) \tag{7}$$

The equation (5) will be :

$$\boxed{\frac{dh}{dx} = \frac{\sqrt{\lambda}}{\mathcal{L}_1}\int_{-\infty}^{x}\frac{h'(u)}{\sqrt{x-u}}du - \frac{\lambda}{\mathcal{L}_2}h(x)} \tag{8}$$

We predict $h(x) = e^{\alpha x}$ a solution to this problem. With $\alpha = a + ib$

$$\Longrightarrow \alpha e^{\alpha x} = \frac{1}{S_1\mathcal{L}_1}\int_{-\infty}^{x}\frac{\alpha e^{\alpha u}}{\sqrt{x-u}}du + \frac{e^{\alpha x}}{S_2\mathcal{L}_2} \tag{9}$$

With S_1 and S_2 are respectively the sign of $\mathcal{L}_1$ and $\mathcal{L}_2$, used positive in the equation above.

$$\Longrightarrow \frac{S_1\sqrt{\mathcal{L}_1}}{\alpha}(\alpha - \frac{1}{S_2\mathcal{L}_2}) = \int_{-\infty}^{0}\frac{e^{\alpha v}}{\sqrt{-v}}dv \tag{10}$$

We know that $\int_{-\infty}^{0}\frac{e^{\alpha v}}{\sqrt{-v}}dv = \frac{\pi}{\alpha}$ for $a > 0$

$$\Longrightarrow \frac{S_1\sqrt{\mathcal{L}_1}}{\sqrt{\alpha}}(\alpha - \frac{1}{S_2\mathcal{L}_2}) = \sqrt{\pi} \tag{11}$$

$\sqrt{\alpha} = c + id$ with $c = \pm\sqrt{\frac{1}{2}(\sqrt{a^2+b^2}+a)}$ and $d = \pm\sqrt{\frac{1}{2}(\sqrt{a^2+b^2}-a)}$

Then the equation (11) would be

$$\begin{cases} \sqrt{\mathcal{L}_1}S_1\sqrt{\frac{1}{2}(\sqrt{a^2+b^2}+a)} = \pi + \frac{S_1}{S_2}\frac{\sqrt{\mathcal{L}_1}}{\mathcal{L}_2}\frac{\sqrt{\frac{1}{2}(\sqrt{a^2+b^2}+a)}}{\sqrt{a^2+b^2}} \\ \sqrt{\mathcal{L}_1}S_1\sqrt{\frac{1}{2}(\sqrt{a^2+b^2}-a)} = -\frac{S_1}{S_2}\frac{\sqrt{\mathcal{L}_1}}{\mathcal{L}_2}\frac{\sqrt{\frac{1}{2}(\sqrt{a^2+b^2}-a)}}{\sqrt{a^2+b^2}} \end{cases} \tag{12}$$

For $b \neq 0$, we have $S_2\mathcal{L}_2\sqrt{a^2+b^2} = -1 \implies \mathcal{L}_2 < 0$ Then $\sqrt{a^2+b^2} = \frac{1}{\mathcal{L}_2}$

$\Longrightarrow 2S_1\sqrt{\mathcal{L}_1}\sqrt{\frac{1}{2}(\frac{1}{\mathcal{L}_2}+a)} = \sqrt{\pi}$

Valid for $S_1 > 0$, $\mathcal{L}_1 > 0$

$$\boxed{\Longrightarrow a = \frac{\pi\mathcal{L}_2 - 2\mathcal{L}_1}{2\mathcal{L}_1\mathcal{L}_2}} \tag{13}$$

a should be positive, $\Longrightarrow \pi\mathcal{L}_2 - 2\mathcal{L}_1 > 0$

$\Longrightarrow \frac{\mathcal{L}_2}{\mathcal{L}_1} > \frac{2}{\pi}$

So we can deduce that for $\mathcal{L}_1 > 0$ and $\mathcal{L}_2 < 0$, the crack path is divergent when $\frac{\mathcal{L}_2}{\mathcal{L}_1} > \frac{2}{\pi}$

The damping length $\xi = \frac{1}{a} = \frac{2\mathcal{L}_1\mathcal{L}_2}{\pi\mathcal{L}_2 - 2\mathcal{L}_1} = \mathcal{L}_1(\frac{1}{R_c - R})$ with $R = \frac{\mathcal{L}_1}{\mathcal{L}_2}$,$R_c = \frac{\pi}{2}$

$b^2 = \frac{1}{\mathcal{L}_2^2} - a^2 = \frac{4\pi^2}{\lambda^2}$ with λ is the wave length of the oscillations of the crack path

$$\boxed{\Longrightarrow \lambda = \frac{4\mathcal{L}_1}{\sqrt{2\frac{R}{R_c} - 1}}} \tag{14}$$

3 Numerical results

We just demonstrated that the crack path follow the equation :

$$\frac{dh}{dx} = \frac{\sqrt{\lambda}}{\mathcal{L}_1} \int_{-\infty}^{x} \frac{h'(u)}{\sqrt{x-u}} du - \frac{\lambda}{\mathcal{L}_2} h(x)$$

We implemented this equation in a matlab program to predict the crack path, we used as a first step $\mathcal{L}_1$ and $\mathcal{L}_2$ constant. We analysed these simulations and we can differentiate four regimes.

- A regime where we have a straight crack path
- A regime where we have a divergent crack path
- A regime where we have damping oscillations
- A regime where we have amplified oscillations

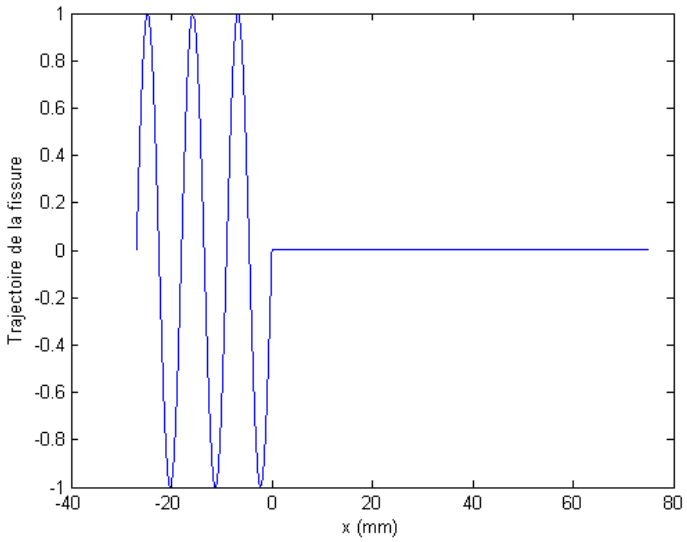

FIGURE 2 – Stable crack path due to a perturbed sinusoidal pre-crack of wave length 12mm, $\mathcal{L}_1$ = 66mm, and $\mathcal{L}_2$ de 20 mm

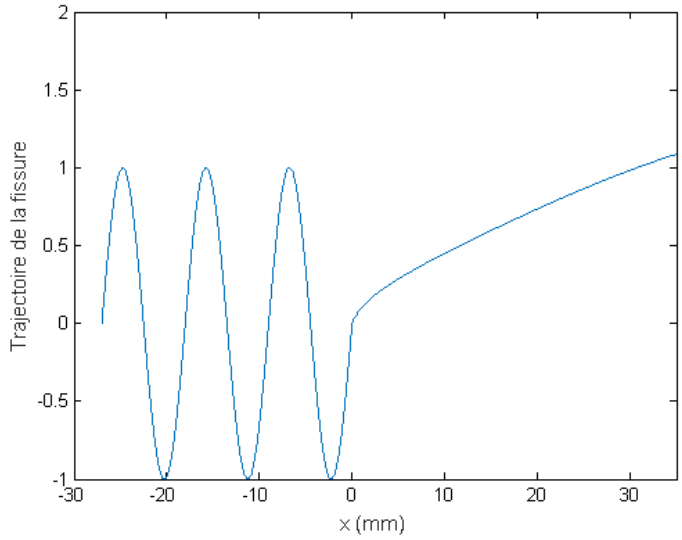

FIGURE 3 – Unstable crack path due to a perturbed sinusoidal pre-crack of wave length 12mm, $\mathcal{L}_1$ = 66mm, and $\mathcal{L}_2$ de 52.5 mm

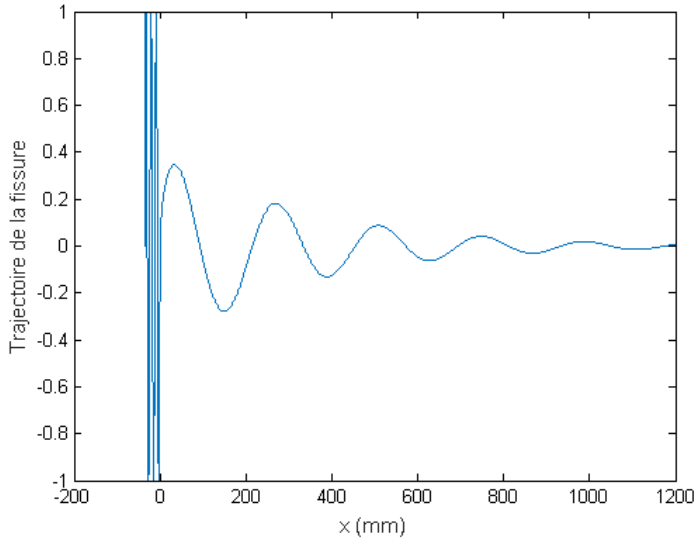

FIGURE 4 – Stable crack path due to a perturbed sinusoidal pre-crack of wave length 12mm, $\mathcal{L}_1$ = 66mm, and $\mathcal{L}_2$ de 37.5 mm

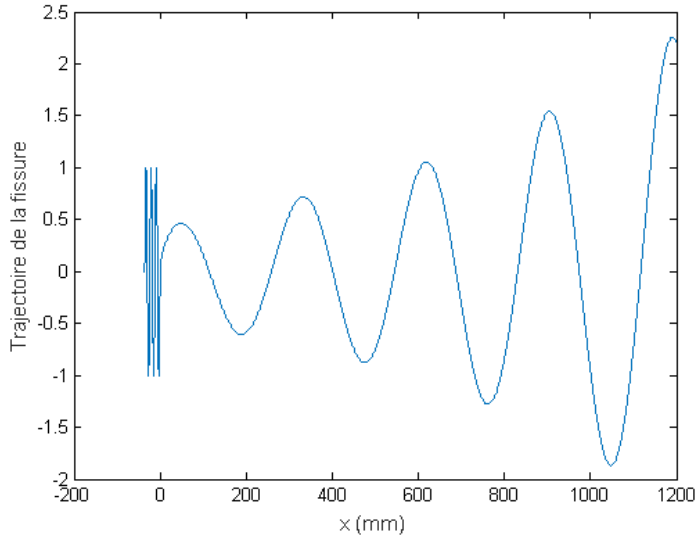

FIGURE 5 – Unstable crack path due to a perturbed sinusoidal pre-crack of wave length 12mm, $\mathcal{L}_1$ = 66mm, and $\mathcal{L}_2$ de 45 mm

To know the difference between these regimes, and the parameters that influence this behavior, we conducted simulations for all possible values of $\mathcal{L}_1$ and $\mathcal{L}_2$. We found the results below :

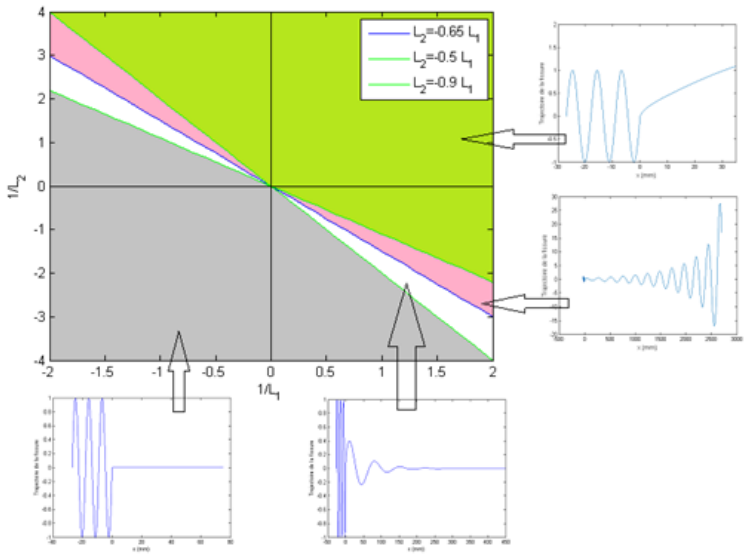

FIGURE 6 – Different regimes of the crack path in function of $\mathcal{L}_1$ and $\mathcal{L}_2$

The difference between the damping regimes and the diverging regimes, is $\frac{\mathcal{L}_2}{\mathcal{L}_1} = 0.65 = \frac{2}{\pi}$ as shown in Figure 6.

These results are totally compatible with the analytical results.

We wanted to compare the damping length and the wave length between the analytical calculations and the numerical simulations, for this we plotted the functions of ξ and λ in both cases. The results are shown in the graphics below.

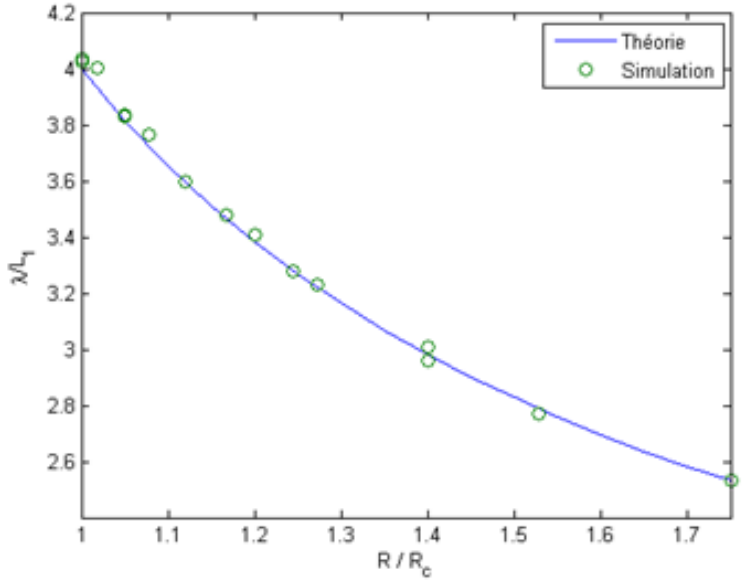

FIGURE 7 – Values of λ in function of $\mathcal{L}_1$,R, and R_c

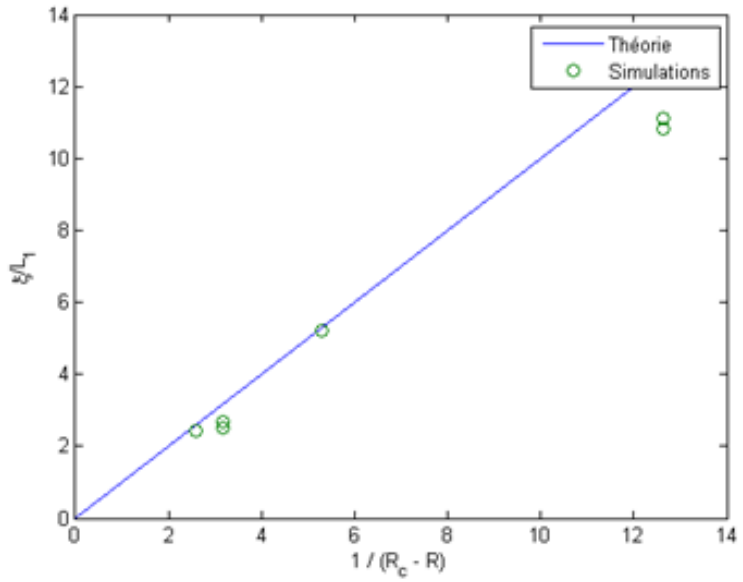

FIGURE 8 – Values of ξ in function of $\mathcal{L}_1$,R, and R_c

4 Experimental results

To compare the experimental and the analytical results, we must have the values of $\mathcal{L}_1$ and $\mathcal{L}_2$. For this purpose we need to calculate the values of $\mathcal{L}_1$ and $\mathcal{L}_2$ of samples may be used during the experiments.

To calculate these terms, we need to evaluate the T-stress T, the A-stress A, and the stress intensity factor K_I for TDCB, and rectangular samples.
We made simulations that give these values, using the finite element calculation software CASTEM. The J-integral method gives the exact value of the stress intensity factor K_I, we extract the values of the stress σ_{xx} in the propagation direction x of the crack at each point on the lip of the crack, and we can find the values of $\mathcal{L}_1$ and $\mathcal{L}_2$ as explained below.

The mesh used is a rectangular mesh in the majority of the sample, with a pitch of 0.25 e_x. This mesh is refined around the crack tip by a distance $\frac{h_1}{5}$ from the 3 sides of the tip. In this rectangle, one has a circle, another finer rectangle, and a second circle even finer with the mesh size of 1E-11 e_x.

This mesh is illustrated in the figure below.

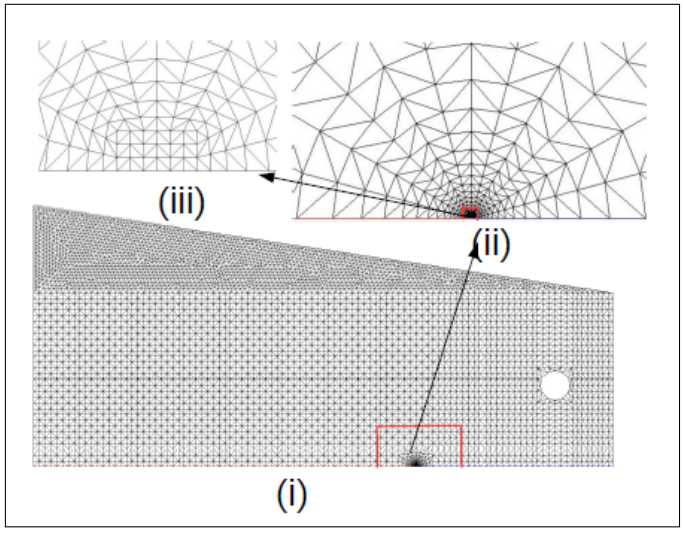

FIGURE 9 – The mesh used in the CASTEM model

On the same graph, we plot the values of σ_{xx} as a function of the distance of the point considered at the crack tip in a logarithmic scale and the values of $\frac{K_I}{sqrt2\Pi r}$ on the same abscissa. These two functions have the same shape, then the following equation is used to measure T and A :

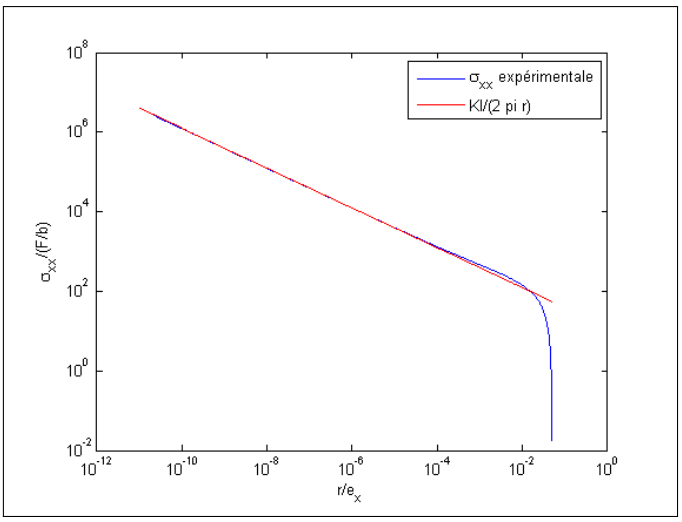

FIGURE 10 – σ_{xx} vs. distance of the point considered at the crack tip in a logarithmic scale

$$\sigma_{xx} = \frac{K_I}{\sqrt{2\pi r}} + T + A\sqrt{r} \tag{15}$$

The graph of $\sigma_{xx} - \frac{K_I}{\sqrt{2\pi r}}$ vs. $\sqrt{r}$ is linear as shown in the graph below, we can calculate the A et le T-stress as the slope and the intersection point of this graph with the y-axis.

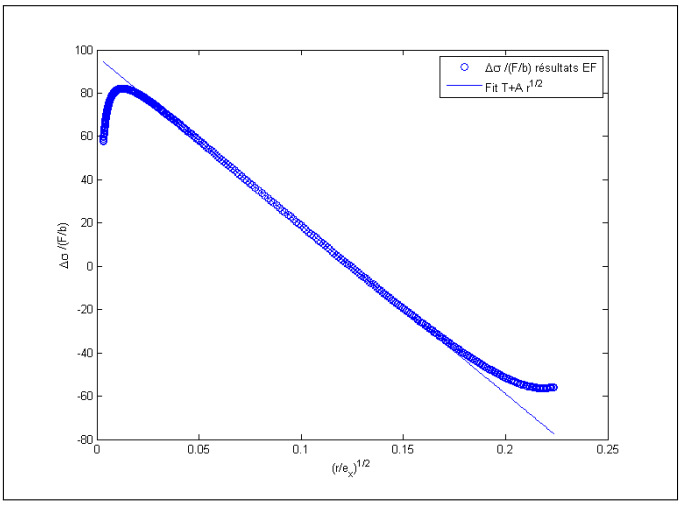

FIGURE 11 – Values of $\sigma_{xx} - \frac{K_I}{\sqrt{2\pi r}}$ as $\sqrt{r}$ varies

After evaluating T and A-stress and k_I, we can calculate $\frac{T}{K_I}$,$\frac{A}{K_I}$,$\mathcal{L}_1$, and $\mathcal{L}_2$. This analysis is repeated for different initial crack length, to know the values of $\mathcal{L}_1$, and $\mathcal{L}_2$, on all the crack path.

We plotted the values of $\mathcal{L}_1$, and $\mathcal{L}_2$ in our reference plane, as shown in the figure below.

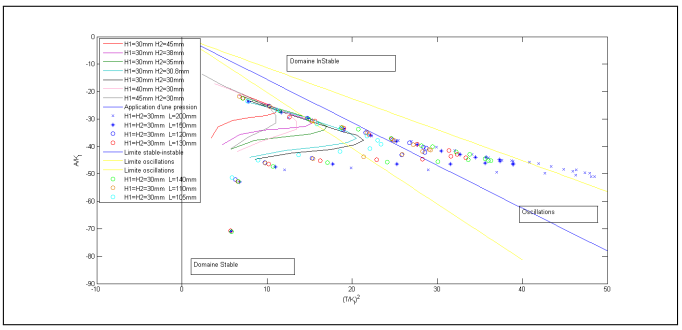

FIGURE 12 – Values of $\mathcal{L}_1$, and $\mathcal{L}_2$ for different sample geometries.

To compare the results, we made traction tests to see the crack path.

The samples used in the experiments are rectangular and TDCB samples of Plexiglas with a perturbed pre-crack made by a laser cutter.

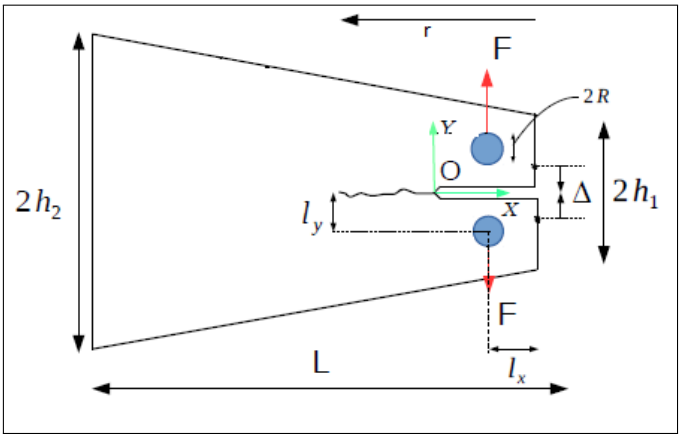

(a) L=100 mm,h1=30 mm, h2=45 mm,l_x=12.8 mm,l_y=14 mm, R=2.5 mm, r=50 mm,Δ=7.5 mm

FIGURE 13 – TDCB sample dimensions

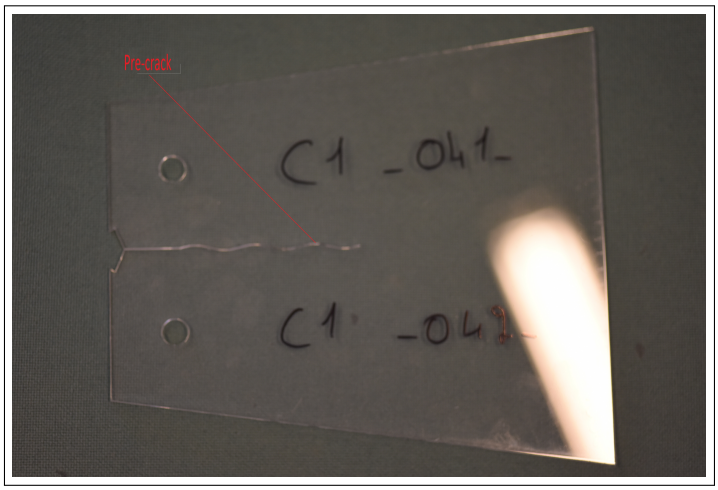

FIGURE 15 – TDCB sample with sinusoidal pre-crack of amplitude 1 mm

The results are compatible with our model as shown in Figure 16.

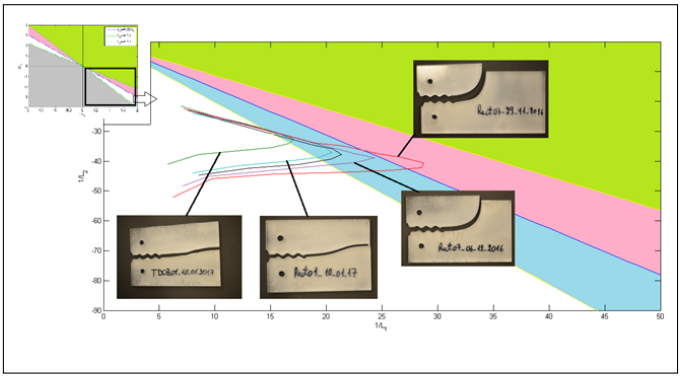

FIGURE 16 – Values of $\mathcal{L}_1$, and $\mathcal{L}_2$ for different sample geometries.

In these experiments we can differentiate the divergent crack paths from the stable ones, but we cannot see the oscillations. This difference is due to the fact that in the simulation we used $\mathcal{L}_1$, and $\mathcal{L}_2$ as constants, but in fact, it's not the case.

Références

[1] B. Cotterell, and J.R. Rice, Slightly curved or kinked cracks, Int. J. Frac. **16**, 155-169 (1980).

[2] A.B. Movchan, On perturbation of plane cracks, Int. J. Solid. **35**, 3419-3453 (1998).

[3] E. Katzav, and M. Adda-Bedia, Stability and roughness of tensile cracks in disordered materials, Physical Review **88**, (2013).

[4] M. Amestoy, and J.B. LeBlond, Crack paths in plane situations - II. Detailed form of the expansion of the stress intensity factors, Int. J. Solids Struct. **29**, 465-501 (1992).